Crossover behaviors in magnetoresistance oscillations for Nb thin film with rectangular arrays of antidots

2012 EPL 99 37006

(http://iopscience.iop.org/0295-5075/99/3/37006)

A Letters Journal Exploring the Frontiers of Physics

August 2012

EPL, **99** (2012) 37006
doi: 10.1209/0295-5075/99/37006

www.epljournal.org

Crossover behaviors in magnetoresistance oscillations for Nb thin film with rectangular arrays of antidots

W. J. Zhang[1(a)], S. K. He[1], H. F. Liu[1], G. M. Xue[1], H. Xiao[1], B. H. Li[1], Z. C. Wen[1], X. F. Han[1], S. P. Zhao[1], C. Z. Gu[1], X. G. Qiu[1(b)] and Victor V. Moshchalkov[2]

[1] *Beijing National Laboratory for Condensed Matter Physics, Institute of Physics, Chinese Academy of Sciences P.O. Box 603, Beijing 100190, PRC*
[2] *INPAC-Institute for Nanoscale Physics and Chemistry, KU Leuven - Celestijnenlaan 200D, B-3001 Leuven, Belgium, EU*

received 18 April 2012; accepted in final form 8 July 2012
published online 8 August 2012

PACS 74.78.Na – Mesoscopic and nanoscale systems
PACS 74.81.Fa – Josephson junction arrays and wire networks
PACS 74.25.F- – Transport properties

Abstract – Superconducting Nb thin films with rectangular arrays of submicron antidots (holes) have been systemically investigated by transport measurements. A series of crossover behaviors is found in magnetoresistance oscillations, corresponding to three different superconducting states: the wire network-like state, the interstitial vortex state and the single-loop–like state. These states are identified by the field intervals and hysteretic effect. The crossover fields between them are found to be both temperature and geometry dependent. Furthermore, in dense arrays, the saturation number is distinctly larger than the theoretical calculation for a single insulating inclusion. Our results indicate that in the process of magnetic field penetration into nanostructured superconductors, the order parameters are strongly modulated and finally localized near the edges, resulting in changes of oscillation modes.

Introduction. – Experiments on nanostructured superconductors with dimensions comparable to the superconducting characteristic length scales have demonstrated that the sample topology strongly influences the superconducting properties, such as the phase boundary $T_c(H)$, the magnetoresistance $R(H)$, and the field-dependent critical current $I_c(H)$ [1–3]. Various topologies (single loops [1,3], large infinite networks [4], and arrays of antidots [5,6]) have been studied both experimentally and theoretically.

In a perpendicular magnetic field, a localized superconducting state can first nucleate near the edge of the samples within a thin layer of width $W_s \sim\xi(T)$, similar to the nucleation of surface superconductivity [7,8]. The so-called edge superconducting state (surface state) [9,10] has an enhanced critical field $H_{c3}(T)$. The enhancement of $H_{c3}(T)$ above the bulk critical field $H_{c2}(T)$ greatly depends on the curvature of the superconducting/normal interface and the surface-to-volume ratio [5,11]. Much higher enhancement of the ratio H_{c3}/H_{c2} up to 3.6 has been observed in Pb thin film with a dense square antidot lattice [11].

For the square arrays of antidots, when the narrowest separation ΔW between neighboring holes is smaller than a critical value $1.84\xi(T)$ [7], nucleation is dominated by the thin wire-like surface states and by the coupling between them. This kind of arrays is well described by the formalism of superconducting wire networks [12,13]. The oscillations of $T_c(H)$ or $R(H)$ in such array are known as collective oscillations or network-like oscillations, whose period is corresponding to the area of the unit cell [4]. As shown by Bezryadin and Pannetier [5], when the magnetic field is high enough, a crossover behavior in the $T_c(H)$ curve from collective oscillations to single-loop–like ("single object") oscillations occurs. The period of the single-loop–like oscillations is determined by the effective area S_{eff} of screening supercurrents,

$$\Phi_0 = \Delta H S_{eff}, \tag{1}$$

where $\Phi_0 = h/2e = 20.7\,\mathrm{G}\,\mu\mathrm{m}^2$ is the flux quantum; ΔH is the period (field interval) of oscillations. Due to the

(a) E-mail: zhangweijun@ssc.iphy.ac.cn
(b) E-mail: xgqiu@iphy.ac.cn

decrease of W_s with increasing magnetic field, the single-loop–like oscillations are non-periodic.

In perforated samples, Abrikosov (interstitial) vortices can appear in the large superconducting segments between the holes, which have been confirmed by imaging techniques [9,10,14,15]. For rectangular arrays of antidots, the interstitial vortices are preferred to reside in wide stripes along the long side when the magnetic field is high enough. Thus, an extra interstitial vortex crossover behavior will be involved in rectangular arrays, in contrast to the one found in the square arrays of antidots [5,6,9].

In this paper, we have performed detailed systematic transport measurements on the rectangular arrays of antidots with various aspect ratios. These array are characterized by the following features: 1) separation ΔW ($\sim 50\,\mathrm{nm}$) of the short side a is smaller than $\xi(T)$; 2) ΔW of the long side b is larger than $4\xi(T)$. We observe successive crossover behaviors from the network-like state to the interstitial vortex state, then to the single-loop–like state, as the magnetic field increases. The hysteretic effect is found for the interstitial vortex state. The crossover fields are strongly dependent on temperature, hole size, and the aspect ratio of the unit cell.

Experiments. – Nb thin films with a thickness of about 100 nm were deposited on $SiO_2(300\,\mathrm{nm})$/Si substrates by magnetron sputtering. The critical temperature T_c of the Nb films is 8.910 K, and the superconducting transition width is about 21 mK (10%–90%R_n criterion, where R_n is the normal state resistance at 9 K). For standard transport measurements, four-probe microbridges were fabricated on the Nb films with ultraviolet photolithography and etched by reactive ion etching (RIE) in O_2 and SF_6 plasmas. The patterned Nb films were then spun with polymethyl metacrylate (PMMA) resist layer and baked at 170 °C for 1 minute. Arrays of circular antidots were written in the central regions ($60\,\mu\mathrm{m} \times 60\,\mu\mathrm{m}$) of the Nb microbridges by electron beam lithography on PMMA resist. The exposed Nb films were developed in MIBK : IPA (1 : 3) solution for 40 seconds. Finally, the samples were etched by RIE again and unexposed PMMA was removed in acetone. Note that one of the Nb microbridges was intentionally unexposed and used as a reference.

Figure 1 shows scanning electron microscope (SEM) and atomic force microscope (AFM) images for sample S1, with a rectangular unit cell of $800\,\mathrm{nm} \times 1200\,\mathrm{nm}$, and a hole radius $r_h = 375\,\mathrm{nm}$. The narrowest separation ΔW between neighboring holes along the X-direction is 50 nm. The images show that the overall periodicity is maintained very well. Sharp edges are obtained after etching.

The measurements were performed in Physical Properties Measurement System (PPMS-14, Quantum Design Inc.). Phase lock-in amplifiers (SR830) were used for ac currents applied at a frequency of 30.9 Hz. The current was parallel to the long side of the rectangular unit cell (the Y-direction). The applied magnetic field was perpendicular to the film surface. We swept the magnetic

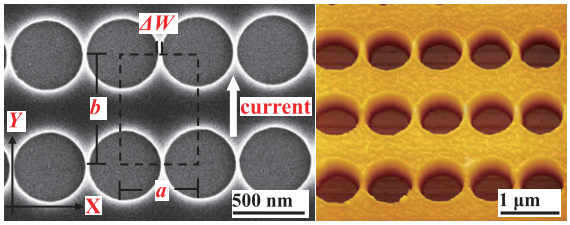

Fig. 1: (Color online) SEM and AFM images of a rectangular antidot lattice (sample S1), with a unit cell of $a \times b$ ($800\,\mathrm{nm} \times 1200\,\mathrm{nm}$). The hole (antidot) radius is 375 nm and the distance between the centers of the holes is 800 nm, resulting in a width ΔW of the narrowest part of the constriction of 50 nm. The dashed rectangle indicates a unit cell.

field with a step of 0.4 Oe in the low-field regime and 1 Oe in the high-field regime. The temperature stability was better than 2 mK during the measurements. The superconducting coherence length $\xi(0)$ is 11.3 nm, and is determined by measuring the $T_c(H)$ of the reference Nb microbridge [16]:

$$H_{c2} = \frac{\Phi_0}{2\pi\xi^2(0)}\left(1 - \frac{T}{T_c}\right). \qquad (2)$$

The penetration depth $\lambda(0)$ is 72.0 nm, derived from the dirty limit ($l < \xi_0$) expressions [17]: $\lambda(0) = 0.85 \times 0.64\,\lambda_L\xi_0/\xi(0)$, where $\xi_0 = 38\,\mathrm{nm}$ is the BCS coherence length, and $\lambda_L = 39\,\mathrm{nm}$ is the London penetration depth. Thus, we have $\xi(t = 0.990) = 113\,\mathrm{nm}$, $\lambda_{eff}(t = 0.990) \approx \lambda^2(t)/d = 1315.6\,\mathrm{nm}$, where $t = T/T_c$ is the reduced temperature, and $d = 100\,\mathrm{nm}$ is the thickness of thin film.

Results and discussion. –

Magnetoresistance and hysteretic effect. The field-dependent $R(H)$ curve for S1 (800×1200, $r_h = 375\,\mathrm{nm}$) at $T = 8.640\,K$ and current $I = 30\,\mu\mathrm{A}$ is given in fig. 2(a). The T_c of S1 is 8.702 K (50%R_n criterion).

Due to the well-defined shape of the dips, we could accurately determine the field intervals ΔH between two consecutive dips (minima). Figure 2(b) shows ΔH as a function of the index number N for S1, at the same temperature $T = 8.640\,\mathrm{K}$. The notation N is a sequence number of dips relative to the one at zero field, which is marked as $N = 0$. The horizontal dashed lines (bottom to top) indicate the average field intervals $\overline{\Delta H}$ in region I, II and III: 20.8 ± 0.5 Oe, 34.9 ± 1 Oe, and 38.1 ± 1 Oe. Thus, three different regimes of the $R(H)$ curve can be distinguished by ΔH: the low-field (region I), the intermediate-field (region II), and the high-field (region III) regimes. It is found that $\overline{\Delta H}$ in the three regions increases with the field. In fig. 2(a), the crossover fields are indicated by the downward arrows at $H_S = 125$ Oe and $H_D = 352$ Oe. It should be noted that, ΔH at $N = 7$ has a value close to the ones in region I, but it belongs to region II. It is related to the formation of the first interstitial vortex in the center of each unit cell.

In the low-field regime ($H < H_S$), $\overline{\Delta H} = 20.8 \pm 0.5$ Oe is relevant to one flux quantum per unit cell. It slightly

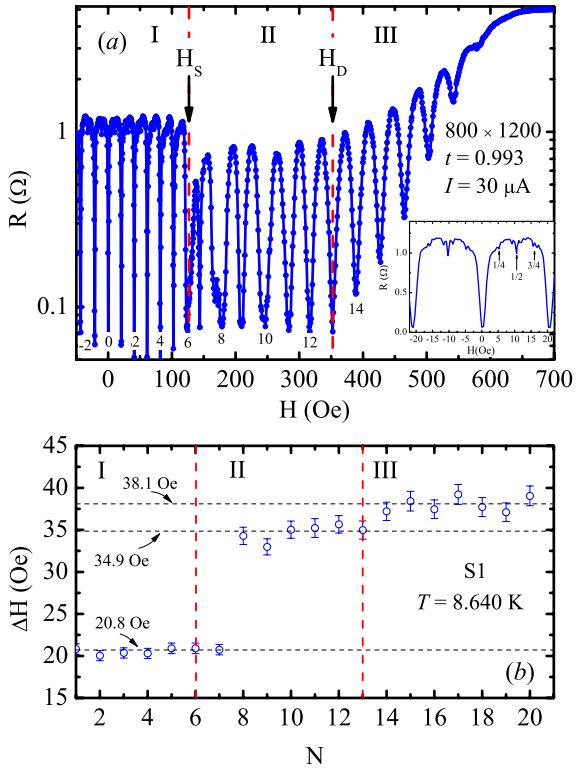

Fig. 2: (Color online) (a) Magnetoresistance of S1 is measured at $T = 8.640$ K ($t = 0.993$) with $I = 30\,\mu$A. The dashed vertical lines divide the $R(H)$ curve into three regions. The downward arrows indicate the crossover fields H_S and H_D. Inset of (a): enlarged plot of the low-field regime. Fractional reduced magnetic fluxes are indicated with upward arrows. (b) Values of the field interval ΔH as a function of the index number N. The dashed horizontal lines indicate the average values of ΔH, corresponding to the three regions in the upper panel: (I) 20.8 Oe, (II) 34.9 Oe, and (III) 38.1 Oe.

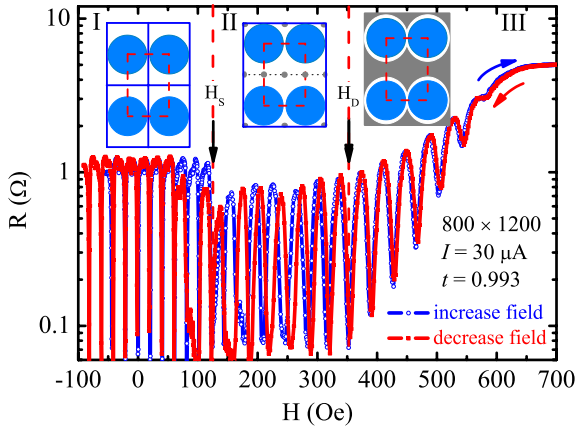

Fig. 3: (Color online) Hysteretic effect of the magnetoresistance for S1. The curves are divided into three parts: (I) $H < H_S$, network-like region, no vortices are located outside the holes; (II) $H_S < H < H_D$, the interstitial vortex sublattice appears in the wide stripes, with a normal core size $\sim 2\xi(T)$; (III) $H > H_D$, the surface state is localized around each hole, forming an elliptical annulus. The insets show schematic drawings of the vortex patterns for each region. The blue disks, the gray spots and the gray regions represent holes, the normal cores of the vortices and normal-state regions, respectively.

deviates from the theoretical value $\Phi_0/ab = 21.6$ Oe. The samples can be described in the framework of the rectangular weak-link wire network, since the separations of neighboring holes is comparable to $\xi(T \sim T_c)$ [4,18–21]. The inset of fig. 2(a) shows a magnification of the low-field $R(H)$ curve. The fractional reduced magnetic flux $f = \Phi/\Phi_0 = (\frac{1}{4},\ \frac{1}{2},\ \frac{3}{4})$ is clearly visible. These features reflect the collective behavior of multiconnected superconducting wire network. A numerical study [22], based on the mean-field Ginzburg-Landau theory for the rectangular wire network, predicts several fractional $f = (\frac{1}{4},\ \frac{1}{3},\ \frac{1}{2}, \ldots)$, which is in a good agreement with our results. Thus, multiconnectivity plays an important role in arrays of large antidots. The description of network-like behavior is different from the arrays with smaller and weaker pinning centers. In the latter case, the observed oscillatory dips in the magnetoresistance were explained by the vortex (multiquanta-vortex) matching model in the London limit [23–28].

The maxima of magnetoresistance show approximately the same magnitude in the low-field regime, suggesting that the multiquanta vortex is effectively confined in each large antidot [9]. When the magnetic field is larger than a saturation field H_S, the $R(H)$ behavior changes drastically. The collective oscillations are interrupted by the formation of additional vortices in the interstitial regions, resulting in broad dips and missing of fine fractional structures. Similar phenomena have also been observed in rectangular arrays of magnetic dots, and explained by the reconfiguration transitions of vortex lattice [24,27].

In the high-field regime ($H > H_D$), a rapid increase of resistance background and a larger $\overline{\Delta H} = 38.1$ Oe is observed. As we will discuss below, the large period oscillations in region III correspond to the single-loop–like behavior. Due to the small separation of neighboring antidots, the screening supercurrents are strongly distorted and redistributed to an elliptical shape [29,30]. Thus, $\Delta H_{SLL} = \Phi_0/S_{eff} = 38.2$ Oe given by eq. (1), is comparable to the experimental value, with

$$\begin{aligned} S_{eff} &= \pi x_m y_m \\ &= \pi(r_h + \Delta W/2)(r_h + \xi(t)/2), \end{aligned} \tag{3}$$

where $r_h = 375$ nm $\Delta W = 50$ nm and $\xi(t = 0.99) = 113$ nm. Note that x_m and y_m are one-half of the ellipse's effective major and minor axes, respectively. This characteristic area depends on $\xi(T)$, because the order parameter has a finite extension $\xi(T)$ at the geometrical edge of the hole. The effective elliptical axis is similar to the mean radius r_m in the Little-Parks effect, where $r_m = (r_o + r_i)/2$ [11], r_o and r_i are the outer and inner loop radius.

In fig. 3, the hysteretic curves are recorded in the following way: the magnetic field first increases from -100 Oe to 750 Oe, then decreases from 750 Oe to -100 Oe. The curves are reversible in regions I and III. In region I,

since only coreless vortices are constraint inside the holes, increasing or decreasing magnetic filed would produce the same magnetoresistance oscillation. In region II, at first, every hole encloses a multiquanta flux ($6\Phi_0$). There is a competition between increasing the flux per hole and accommodating vortices at interstitial positions in the wide stripes. The additional vortices are energetically favorable to appear in the weak superconducting regions. Furthermore, the interstitial vortices in the wide stripes can form stable sublattices, which produce dips in the $R(H)$ curves [25,26]. Then, a larger $\overline{\Delta H}$ (34.9 Oe) illustrates the existence of a dense vortex distribution, in contrast to region I. This field interval is comparable with the theoretical expectation for the reconfiguration of the square lattice $\Delta \mathrm{H}_{Sq} = \Phi_0/a^2 = 32.3$ Oe [24,27], where $a =$ 800 nm. Normally, the hysteretic effect implies the existence of a surface barrier or a surface pinning effect (flux trapped by random defects) for vortex motion [31,32]. To our samples, since the measured temperatures is close to T_c, the flux pinning force is quite weak and negligible. Thus, the hysteretic effect in region II may be caused by a surface barrier between the three regimes, related to a first-order transition. Indeed, for the multiquanta vortex (coreless vortices) to interstitial vortices, a surface barrier (ψ-barrier) for vortex entrance and exit will lead to a first-order phase transition [33], which could explain the hysteretic effect in magnetoresistance.

With increasing field, the vortex patterns become complex, and parts of the interstitial regions turn into normal state due to the penetration of the magnetic field. In region III, most of the regions in S1 turn to normal states, except that surface states around holes are still superconducting (see the inset of fig. 3). The curves become reversible again. A synchronized entrance of an additional vortex in each hole causes a resistance minimum in $R(H)$, like the Little-Parks effect [1].

From the hysteresis measurements, the boundaries of three regions can be clearly distinguished. The same conclusions can also be obtained from sample S2 ($a =$ 800 nm, $b = 2000$ nm, $r_h = 373$ nm), with $H_S = 39$ Oe and $H_D = 319$ Oe at $T = 8.640$ K. In contrast to the work on magnetic dots [27], the hysteresis curves were measured just above or below the transition field, and then the divisions of the three regimes were possibly missed in their discussion.

Parameters affecting the crossover fields. Figure 4 shows the $R(f)$ curves of samples S1 and S2 measured at several temperatures, with $I = 30$ μA (panel (a)) and 200 μA (panel (b)), respectively. Since these two samples show a very similar temperature dependence of the $R(f)$ curves, we focus our discussion on S1. In fig. 4(a), from top to bottom, the temperature decreases from 8.723 K to 8.540 K (some curves are not shown in the figure). In the network-like region of the $R(f)$ curves, integer dips are always visible at these temperatures. Even some dips at fields ($f = \frac{1}{4}$, $\frac{1}{3}$, $\frac{1}{2}$) are well developed when the temperature is lower than 8.680 K. However, the

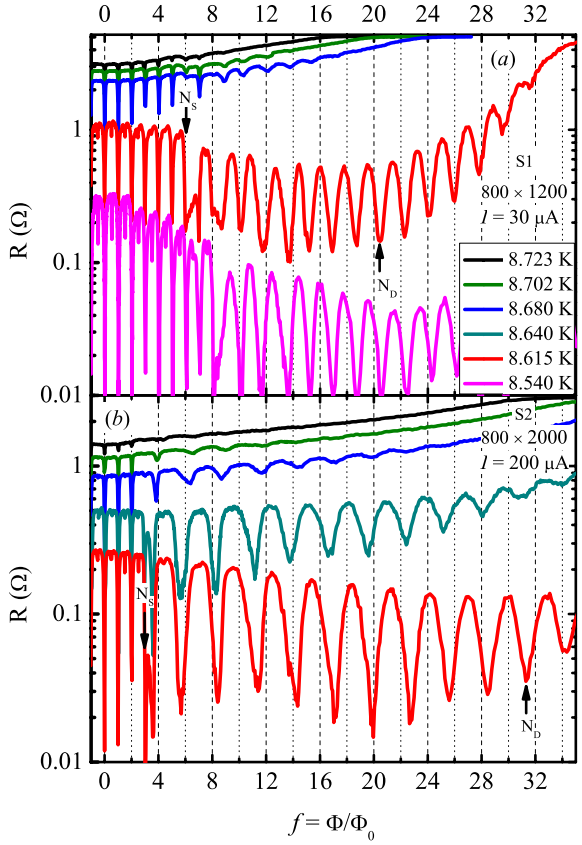

Fig. 4: (Color online) Resistance as a function of reduced magnetic flux f for S1 (upper panel (a)) and S2 (lower panel (b)), measured at several temperatures with fixed currents $I = 30\,\mu$A and $200\,\mu$A, respectively. From top to bottom, the corresponding temperatures of $R(f)$ curves are 8.723 K, 8.702 K, 8.680 K, 8.615 K and 8.540 K (some curves are not shown in the figures).

magnetoresistance oscillations in the intermediate region and single-loop–like region are very sensitive to temperature variation. At high temperatures close to T_c ($T > 8.680$ K), the oscillations in these two regions are broad and shallow. With decreasing temperature, the oscillations become more pronounced. As the temperature further decreases ($T < 8.540$ K, not shown), the oscillations become weaker and finally disappear. This illustrates the different oscillation nature in these three regions.

The saturation number N_S is defined by the largest possible number of the flux quanta trapped by an antidot. Mkrtchyan and Shmidt [34] had theoretically estimated the maximum possible number of vortices trapped by a single insulating inclusion with an expression of $N_{St}(t) = r_h/2\xi(t)$.

In our case, larger hole and smaller separation of antidots along the X-direction are both used, where the surface superconductivity is more significant and produces effective constraint to the flux [9,10]. As indicated by the arrow in fig. 4(a), $N_S = 6$ at $T = 8.615$ K. It is larger than the theoretical value $N_{St}(t = 0.99,\, r_h = 375\,\mathrm{nm}) \sim 2$.

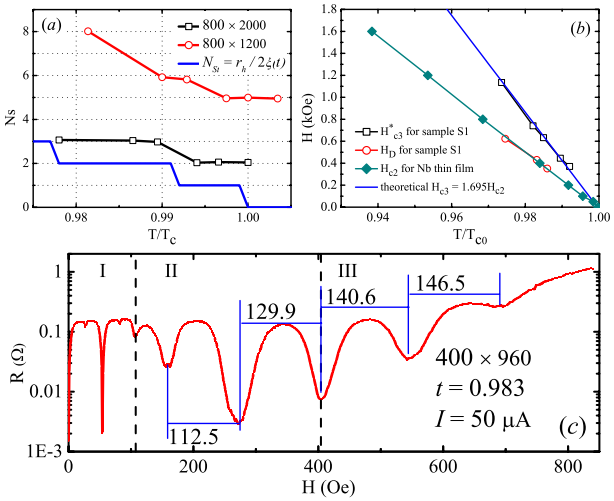

Fig. 5: (Color online) (a) Temperature dependence of the saturation numbers N_S for sample S1 and S2, contrasted with the theoretical values $N_{St}(t) = r_h/2\xi(t)$. (b) Phase boundary for arrays of antidots and a reference Nb thin film. H_{c3} is calculated with $1.695H_{c2}$, where H_{c2} is the experimental data for the Nb thin film. H^*_{c3} is the experimental data obtained from the $90\%R_n$ criterion in fig. 4(a). (c) The $R(H)$ curve for the sample D1 with a rectangular array of antidots (400 nm × 960 nm) is measured at $t = 0.983$ with $I = 50\,\mu$A.

In fig. 5(a), values of N_S as a function of temperature for these two samples are compared with $N_{St}(t)$. As the temperature decreases, N_S increases stepwisely. Interestingly, the experimental result for S2 is closer to the theoretical value at low temperature ($N_S \approx 3$, at $t = 0.978$). This is due to the fact that the distributions of antidots in S2 are sparser along the Y-direction (or have a larger aspect ratio b/a). In contrast, N_S for S1 is nearly 2–3 times of that for S2 at the same reduced temperature. This also the greatest difference between S1 and S2. Normally, in an array of antidots, the antidot-vortex interaction strongly affects N_S, resulting in a larger saturation number in the dense array [35,36]. Besides, the hole size [18,19], and magnetic field [18] are also influencing N_S. Therefore, the transition between region I and II is mainly determined by the saturation number N_S, which is temperature, geometry and magnetic field dependent.

In fig. 5(b), we plotted another crossover field H_D *vs.* the reduced temperature t, and obtained a linear temperature dependence $H_D(t)$. It is found that $H_D(t)$ nearly coincides with the experimental $H_{c2}(t)$ for the Nb thin film. Using eq. (2), we can roughly estimate the upper critical field for the Nb thin film. The theoretical value $H^*_{c2}(T/T_{c0} = 0.986) = 361$ Oe is close to the value of $H_D = 352$ Oe at $T = 8.640$ K, where $T_{c0} = 8.763$ K is obtained from a linear extrapolation of $H_D(t)$ to zero field. This suggests that H_D can be identified as H_{c2} of sample S1. The enhanced H^*_{c3} is also near the value of $1.695\,H_{c2}$ [7], where H^*_{c3} is $90\%R_n$ for the $R(H)$ curves in fig. 4(a). The region between H_{c3} and H_{c2} is the region where the bulk sample is already in the normal state and only a surface state persists. When the temperature is below 8.640 K in fig. 4(a), we notice a decrease of the resistance maxima in a wide range of the magnetic field. This abnormal effect is related to the surface superconductivity around hole edges and it reaches its maximum near H_{c2} (corresponding to H_D) [37]. As the surface states merge with wide stripes containing a finite value of the order parameter, the whole array re-enters into the superconducting state. This has been found in $T = 8.540$ K for S2 (not shown in the figure).

By comparing the $R(H)$ curves of S1 with those of S2, we can study the influence of the geometry (aspect ratio) on the magnetoresistance oscillation. However, there is no much difference in the position of the fine structures in the low-field regime or the position of dips in the high-field regime, except the difference in H_S and H_D. This implies that the oscillations in the $R(H)$ curves are mainly influenced by the connectivity and the upper critical fields of the arrays.

Discussion. To further confirm our observations, samples with smaller unit cells are fabricated to obtain a larger ΔH in $R(H)$ curves. The results for sample D1 (400×960, $r_h = 170$ nm) are illustrated in fig. 5(c). In the range of 272 Oe $< H <$ 402 Oe, values of ΔH agree with the period of square lattice $\Delta H_{Sq} = \Phi_0/a^2 = 129.4$ Oe, where $a = 400$ nm. When $H > 405$ Oe, $\overline{\Delta H}$ is equal to 143.6 Oe, which is close to the calculated value $\Delta H_{SLL} = 145.5$ Oe for the single-loop–like oscillations, with an area of the ellipse $S_{eff} = \pi \times 200\,\text{nm} \times 226.5\,\text{nm}$. Similar results are also obtained in other samples (*e.g.*, 400×655, 400×800 and 400×1000).

Finally, we compare our results with previous works. Firstly, in contrast to the square arrays of antidots, an extra transition (interstitial vortex state) between collective oscillations and single-loop–like oscillations is found at the saturation field H_S. At higher fields, it indicates that the crossover from the interstitial vortex state to the single-loop–like state is triggered by the upper critical field of the sample. Our experiments offer an indirect way to study the process of magnetic field penetration. Moreover, in the analysis of the vortex confinement effect for the large antidots near H_{c2}, it is important to take into account the strong non-uniformity of the order parameters.

Secondly, changes in the periodicity and the shape of the dips in magnetoresistance have been found in superconductors with magnetic dots, nonmagnetic dots and antidots [24,27]. The dominant mechanisms discussed in those works are analyzed in terms of two possible models: the reconfiguration model and the multivortex model. Following these pictures, our results require that vortices form a denser state in the high-field region. However, there are difficulties with the explanation of the phenomena, such as the periodic appearances of the fine structures in region I, the non-hysteretic effects in region III and the very large field intervals (40 Oe $> \Delta H_{Sq}$, for S1) at fields higher than the upper critical field. On the other hand, from the viewpoint of the dynamics of the vortex lattice ordering [38], a monotonic increase in the intervals with increasing magnetic field is

supposed to occur. However, this has not been found in our work. Thus, it seems to be inappropriate to use the London limit at such high temperatures and magnetic fields. We can discuss the results in the framework of the Ginzburg-Landau theory by considering the order parameter modulation. To clarify these effects, further direct imaging experiments, transport measurements and theoretical simulations in such arrays are necessary.

Conclusion. – In conclusion, we have investigated the magnetoresistance of superconducting Nb thin films containing rectangular arrays of large antidots. The $R(H)$ curve is divided into three regions by comparing the results with hysteresis measurements. At low magnetic fields, the system behaves like a weak-link wire network, giving rise to dips in $R(H)$ at integral and fractional reduced magnetic flux below the saturation field H_S. At the intermediate fields, the interstitial vortices form sublattices, leading to larger magnetic field intervals and a hysteretic effect in the $R(H)$ curves. As soon as the magnetic field exceeds H_{c2}, the surface superconductivity nucleates near the edge of the antidot, resulting in a single-loop–like superconducting state. In this state, the non-periodic oscillations and a fully reversible behavior are found in the $R(H)$ curves. The crossover fields (H_S and H_{c2}) among the three regions are found to be geometry and temperature dependent. These observations suggest that the order parameters of the nanostructured superconductors are greatly modulated, especially at the temperature or magnetic field near the critical value.

* * *

We thank Q. Niu, X. C. Xie, and F. Nori for fruitful discussions. WJZ gratefully acknowledges the help of microfabrication Lab and thanks S. K. Su of group EX2 in IOP, CAS. This work is supported by National Basic Research Program of China (Nos. 2009CB929102, 2011CBA00107, 2012CB921302) and National Science Foundation of China (Nos. 10974241, 91121004, 11104335). The work in the KU Leuven is supported by the Methusalem Funding by the Flemish Government.

REFERENCES

[1] Little W. A. and Parks R. D., *Phys. Rev. Lett.*, **9** (1962) 9.
[2] Moshchalkov V. V., Gielen L., Strunk C. *et al.*, *Nature*, **373** (1995) 319.
[3] Berdiyorov G. R., Yu S. H., Xiao Z. L., Peeters F. M., Hua J., Imre A. and Kwok W. K., *Phys. Rev. B*, **80** (2009).
[4] Pannetier B., Chaussy J., Rammal R. and Villegier J. C., *Phys. Rev. Lett.*, **53** (1984) 1845.
[5] Bezryadin A. and Pannetier B., *J. Low Temp. Phys.*, **98** (1995) 251.
[6] Rosseel E., Puig T., Baert M. *et al.*, *Physica C*, **282** (1997) 1567.
[7] Saint-James D. and de Gennes P. G., *Phys. Lett.*, **7** (1963) 306.
[8] Ning Y., Song C., Guan Z., Ma X., Chen X., Jia J. and Xue Q., *EPL*, **85** (2009) 27004.
[9] Bezryadin A. and Pannetier B., *J. Low Temp. Phys.*, **102** (1996) 73.
[10] Veauvy C., Hasselbach K. and Mailly D., *Phys. Rev. B*, **70** (2004) 214513.
[11] Berger J. and Rubinstein J. (Editors), *Connectivity and Superconductivity* (Springer-Verlag, Berlin) 2000, pp. 87–137.
[12] Alexander S., *Phys. Rev. B*, **27** (1983) 1541.
[13] Rammal R., Lubensky T. C. and Toulouse G., *Phys. Rev. B*, **27** (1983) 2820.
[14] Karapetrov G., Fedor J., Iavarone M., Rosenmann D. and Kwok W. K., *Phys. Rev. Lett.*, **95** (2005) 167002.
[15] Kramer R. B. G., Silhanek A. V. and Van de Vondel J. *et al.*, *Phys. Rev. Lett.*, **103** (2009) 067007.
[16] Tinkham M., *Introduction to Superconductivity*, 2nd edition (McGraw-Hill, New York) 1996, p. 135.
[17] de Gennes P. G., *Superconductivity of Metals and Alloys* (Addison-Wesley, New York) 1989, p. 225.
[18] Moshchalkov V. V., Baert M., Metlushko V. V. *et al.*, *Phys. Rev. B*, **57** (1998) 3615.
[19] Hoffmann A., Prieto P. and Schuller I. K., *Phys. Rev. B*, **61** (2000) 6958.
[20] Patel U., Xiao Z. L., Hua J. *et al.*, *Phys. Rev. B*, **76** (2007) 020508.
[21] He S. K., Zhang W. J., Liu H. F. *et al.*, *J. Phys.: Condens. Matter.*, **24** (2012) 155702.
[22] Hu C.-R. and Chen R. L., *Phys. Rev. B*, **37** (1988) 7907.
[23] Reichhardt C., Olson C. J. and Nori F., *Phys. Rev. Lett.*, **78** (1997) 2648.
[24] Martín J. I., Vélez M., Hoffmann A., Schuller I. K. and Vicent J. L., *Phys. Rev. Lett.*, **83** (1999) 1022.
[25] Metlushko V., Welp U., Crabtree G. W. *et al.*, *Phys. Rev. B*, **60** (1999) R12585.
[26] Reichhardt C., Zimányi G. T. and Grønbech-Jensen N., *Phys. Rev. B*, **64** (2001) 014501.
[27] Stoll O. M., Montero M. I., Guimpel J., Åkerman J. J. and Schuller I. K., *Phys. Rev. B*, **65** (2002) 104518.
[28] Kemmler M., Gürlich C., Sterck A., Pöhler H., Neuhaus M., Siegel M., Kleiner R. and Koelle D., *Phys. Rev. Lett.*, **97** (2006) 147003.
[29] Velez M., Jaque D., Martín J. I., Montero M. I., Schuller I. K. and Vicent J. L., *Phys. Rev. B*, **65** (2002) 104511.
[30] Wördenweber R., Dymashevski P. and Misko V. R., *Phys. Rev. B*, **69** (2004) 184504.
[31] Bean C. P., *Phys. Rev. Lett.*, **8** (1962) 250.
[32] Zeldov E., Clem J. R., McElfresh M. and Darwin M., *Phys. Rev. B*, **49** (1994) 9802.
[33] Bezryadin A. and Pannetier B., *J. Low Temp. Phys.*, **102** (1996) 73.
[34] Mkrtchyan G. and Shmidt V., *Sov. Phys. JETP*, **34** (1972) 195.
[35] Doria M., de Andrade S. and Sardella E., *Physica C*, **341** (2000) 1199.
[36] Berdiyorov G. R., Milošević M. V. and Peeters F. M., *Phys. Rev. B*, **74** (2006) 174512.
[37] Fink H., *Phys. Rev. Lett.*, **14** (1965) 309.
[38] Kokubo N., Besseling R., Vinokur V. M. and Kes P. H., *Phys. Rev. Lett.*, **88** (2002) 247004.